Supporting Information

TABLE OF CONTENTS

EXPERIMENTAL SECTION

Materials and methods. Unless otherwise noted, all manipulations were carried out at room temperature under an atmosphere of argon in a glovebox (Vigor) or using Schlenk techniques. Tetrahydrofuran (THF), toluene and hexane were dried via solvent purification system (Braun). $Et_3N \cdot HF$ was obtained by mixing $Et_3N \cdot 3HF$ with two equivalents of Et_3N. [Cp'$_3$Dy] was prepared according to the literatures with some modification. All other reagents were commercially available and used as received. Elemental analysis was performed by Elementar Vario MICRO CUBE (Germany).

X-ray crystallography

All crystals were manipulated under a nitrogen atmosphere and covered in grease. Data collections were performed at 180 K on an Agilent technologies Super Nova Atlas Dual System, with a (Mo Kα= 0.71073 Å) microfocus source and focusing multilayer mirror optics. The structures were solved by direct methods and refined with the full-matrix least-squares technique based on F^2 using the Olex2 program.[1] All non-hydrogen atoms were refined anisotropically. All hydrogen atoms were placed at the calculation positions. The disordered solvent molecules were squeezed using the PLATON program.[2]

Magnetic measurement

Samples were fixed by N-grease to avoid moving during measurement. Direct current susceptibility experiment was performed on Quantum Design MPMS XL-5 SQUID magnetometer on polycrystalline samples. Alternative current susceptibility measurements with frequencies ranging from 100 to 10000 Hz were performed on Quantum Design PPMS. All dc susceptibilities were corrected for diamagnetic contribution from the sample holder, N-grease and diamagnetic contributions from the molecule using the pascal's constants.

1Dy: A THF solution (10 mL) of $Et_3N{\cdot}HF$ (42.2 mg, 0.348 mmol) was added into the solution of [Cp'$_3$Dy] (200 mg, 0.348 mmol) in THF under -20℃ and stirred for 24 h. The precipitates were filtered and collected. The raw product was dissolved in 2 mL toluene, stored under -25℃ for several days, yielding crystals. Yield: 54 mg. Anal. Calcd (%) for $C_{48}H_{74}F_3Si_6Dy_3(C_7H_8)$: C, 45.36; H, 5.67. Found: C, 45.82; H, 5.78.

2Dy: The preparing method was similar to **1Dy**. The raw product was dissolved in hexane and recrystallized under -25℃. Anal. Calcd (%) for $C_{56}H_{94}F_6Si_6Dy_4O_2(C_6H_{14})$: C, 40.96; H, 5.99. Found: C, 40.61; H, 5.74.

3Dy: The preparing method was similar to **2Dy**, where the molar ratio of [Cp'$_3$Dy] and $Et_3N{\cdot}HF$ was changed to 1:1.5. Anal. Calcd (%) for $C_{64}H_{110}F_{15}Si_6Dy_7O_4(C_6H_{14})$: C, 32.08; H, 4.77. Found: C, 31.55; H, 4.51.

4Dy: A toluene solution (10 mL) containing 0.610 mmol of H_2O was slowly added to the solution of [Cp'$_3$Dy] (350 mg, 0.610 mmol) in toluene under -20℃ and stirred overnight. The precipitates were collected by filtration and dried under vacuum. Then the solid was dissolved in 2 mL toluene and stored under -25℃ for several days to yield colorless single crystals. Yield: 83 mg. Anal. Calcd (%) for $C_{32}H_{54}Si_4Dy_2O_2$: C, 42.75; H, 6.12. Found: C, 42.32; H, 5.99.

***Ab initio* calculations**

The two, one and four types of Dy^{III} fragments of complexes **1Dy**,**2Dy** and **4Dy** were calculated, respectively. Complete-active-space self-consistent field (CASSCF) calculations on individual Dy^{III}

fragments of the model structures extracted from the compound on the basis of single-crystal X-ray determined geometry have been carried out using MOLCAS 8.2 program package.[3] Each Dy^{III} fragment was calculated with experimentally determined structure of the corresponding compound while replacing the other Dy^{III} ions by diamagnetic Lu^{III} ions. The basis sets for all atoms are atomic natural orbitals from the MOLCAS ANO-RCC library: ANO-RCC-VTZP for Dy^{III} ion; VTZ for close C and O in **4Dy**, C and F in **1Dy** and **2Dy**; VDZ for distant atoms. The calculations employed the second order Douglas-Kroll-Hess Hamiltonian, where scalar relativistic contractions were taken into account in the basis set and the spin-orbit couplings were handled separately in the restricted active space state interaction (RASSI-SO) procedure. For individual Dy^{III} fragment, active electrons in 7 active spaces include all *f* electrons (CAS (9 in 7)) in the CASSCF calculation. To exclude all the doubts, we calculated all the roots in the active space. We have mixed the maximum number of spin-free state which was possible with our hardware (all from 21 sextets, 128 from 224 quadruplets, 130 from 490 doublets). Single−Aniso program was used to obtain energy levels, ***g*** tensors, m_J values, magnetic axes, etc. based on the above CASSCF/RASSI calculations.[4,5]

Table S1: Crystallographic data and refinement for complexes **1-4**.

	1Dy	**2Dy**	**3Dy**	**4Dy**
Formula	$C_{48}H_{74}Dy_3F_3Si_6\cdot(C_7H_8)$	$C_{56}H_{94}Dy_4F_6O_2Si_6\cdot(C_6H_{14})$	$C_{64}H_{110}Dy_7F_{15}O_4Si_6\cdot(C_6H_{14})$	$C_{32}H_{54}Dy_2O_2Si_4$
Mr	1456.25	1818.02	2620.72	908.11
cryst syst	triclinic	monoclinic	Triclinic	monoclinic
space group	$P\bar{1}$	$P2_1/c$	$P\bar{1}$	$P2_1/c$
a, Å	12.1349(4)	13.8238(3)	14.4849(3)	13.1068(2)
b, Å	12.1825(3)	25.4525(6)	16.1855(4)	23.7324(3)
c, Å	22.6447(7)	22.0905(5)	20.3478(4)	25.4803(5)
α, deg	81.832(2)	90	76.1439(19)	90
β, deg	74.493(3)	90.064(2)	75.9937(18)	102.1981(17)
γ, deg	69.021(3)	90	78.922(2)	90
V, Å^3	3007.96(17)	7772.5(3)	4448.10(18)	7746.9(2)
Z	2	4	2	8
T, K	180	180	180	180
μ, mm^{-1}	3.844	3.939	5.952	3.976
λ, Å	0.71073	0.71073	0.71073	0.71073
GOF	1.055	1.056	1.070	1.128
R_{int}	0.0574	0.0729	0.0453	0.0576
R_1, $wR_2[I > 2\sigma(I)]$	0.0346, 0.0678	0.0545, 0.1333	0.0327, 0.0578	0.0340, 0.0667
R_1, wR_2[all data]	0.0546, 0.0781	0.0781, 0.1535	0.0598, 0.0683	0.0556, 0.0770

Table S2: Selected Distances (Å) and Angles (°) for complex **1Dy**.

	Dy1	Dy2	Dy3
Dy–F	(F1)2.204(2)	(F1)2.195(2)	(F2)2.202(2)
Dy–F	(F3)2.197(2)	(F2)2.206(2)	(F3)2.201(2)
Dy–C(Cp'1)	2.667 (5)	2.631(5)	2.651(5)
	2.680(5)	2.630(5)	2.670(5)
	2.642(5)	2.651(5)	2.625(5)
	2.645(5)	2.659(5)	2.641(5)
	2.681(5)	2.654(5)	2.681(5)
Average	2.663(5)	2.645(5)	2.653(5)
Dy–C(Cp'2)	2.667(5)	2.651(5)	2.653(5)
	2.636(5)	2.657(5)	2.658(5)
	2.634(5)	2.649(5)	2.669(5)
	2.647(5)	2.658(5)	2.647(5)
	2.661(5)	2.654(5)	2.652(5)
Average	2.649(5)	2.654(5)	2.656(5)
Angle of F-Dy-F	86.2(1)	87.5(1)	85.9(1)
Angle of Centroid(Cp'1)-Dy-Centroid(Cp')	130.8(1)	130.5(1)	129.6(1)
Dihedral angle of the two Cp'	50.8(1)	50.1(1)	50.6(1)

Angle of Dy-F-Dy	Dy1-F-Dy2	Dy2-F-Dy3	Dy1-F-Dy3
	152.0(6)	154.3(0)	152.4(6)

Table S3: Selected Distances (Å) and Angles (°) for complex **2Dy**.

	Dy3	Dy4
Dy–F	(F3)2.191(6)	(F6)2.199(6)
Dy–F	(F4)2.172(5)	(F5)2.195(5)
Dy–C(Cp'1)	2.678(1)	2.645(1)
	2.644(1)	2.657(1)
	2.662(1)	2.672(1)
	2.670(1)	2.697(1)
	2.663(1)	2.650(1)
Average	2.663(1)	2.664(1)
Dy–C(Cp'2)	2.677(1)	2.682(1)
	2.678(1)	2.669(1)
	2.658(1)	2.646(1)
	2.658(1)	2.680(1)
	2.645(1)	2.681(1)
Average	2.663(1)	2.671(1)
Angle of F-Dy-F	90.6(1)	88.4(1)
Angle of Centroid(Cp')-Dy-Centroid(Cp')	131.6(1)	128.3(1)
Dihedral angle of the two Cp'	48.7(1)	50.5(1)

	Dy2		Dy1
Dy–F4	2.232(6)	Dy–F3	2.219(6)
Dy–F6	2.251(6)	Dy–F5	2.228(6)
Dy–F1	2.242(5)	Dy–F1	2.268(5)
Dy–F2	2.223(5)	Dy–F2	2.204(5)
Dy–O1	2.396(7)	Dy–O10	2.409(6)
Dy–Cp'	2.706(1)	Dy–Cp'	2.728(1)
	2.707(1)		2.709(1)
	2.698(9)		2.704(1)
	2.683(1)		2.687(1)
	2.707(1)		2.710(1)
Average	2.700(1)	average	2.707(1)
Angle of F1-Dy2-Cp'	170.9(1)	Angle of F1-Dy1-Cp'	173.6(1)

Angle of Dy-F-Dy	Dy3-F4-Dy2	Dy2-F6-Dy4	Dy4-F5-Dy1	Dy1-F3-Dy3
	142.9(3)	143.6(3)	143.1(3)	141.0(3)

Table S4: Selected Distances (Å) and Angles (°) for complex **3Dy**.

	Dy1
Dy–F1	2.274(3)
Dy–F5	2.268(3)
Dy–F6	2.340(2)
Dy–C(Cp’1)	2.668(5)
	2.665(5)
	2.675(5)
	2.685(5)
	2.671(5)
Average	2.672(5)
Dy–C(Cp’2)	2.670(5)
	2.667(5)
	2.687(5)
	2.684(5)
	2.684(5)
Average	2.678(5)
Angle of F1-Dy-F5	133.9(1)
Angle of Centroid(Cp’)-Dy-Centroid(Cp’)	135.5(1)
Dihedral angle of the two Cp’	43.7(1)

	Dy2		Dy5
Dy–F1	2.186(2)	Dy–F4	2.194(2)
Dy–F2	2.190(2)	Dy–F5	2.187(2)
Dy–F6	2.308(3)	Dy–F6	2.299(3)
Dy–F7	2.183(2)	Dy–F10	2.189(2)
Dy–F11	2.195(2)	Dy–F14	2.181(2)
Dy–O81	2.403(4)	Dy–O90	2.400(4)
Dy–O85	2.370(5)	Dy–O75	2.375(3)
	Dy3		Dy4
Dy–F2	2.208(2)	Dy–F3	2.194(3)
Dy–F3	2.196(3)	Dy–F4	2.213(2)
Dy–F8	2.197(2)	Dy–F9	2.206(2)
Dy–F12	2.207(2)	Dy–F13	2.191(2)
Dy–F15	2.550(3)	Dy–F15	2.515(3)
Dy–Cp’	2.654(7)	Dy–Cp’	2.678(7)
	2.672(7)		2.663(7)
	2.645(7)		2.662(7)
	2.663(7)		2.659(7)
	2.666(7)		2.664(7)

Average	2.660(7)		2.665(7)
Angle of F15-Dy-Cp’	178.1(1)	Angle of F15-Dy-Cp’	177.7(1)
	Dy6		Dy7
F7	2.190(3)	F11	2.191(2)
F8	2.192(3)	F12	2.190(3)
F9	2.197(2)	F13	2.193(3)
F10	2.184(2)	F14	2.190(3)
F15	2.815(2)	F15	2.695(2)
Cp’	2.649(6)	Cp’	2.656(6)
	2.629(6)		2.679(6)
	2.664(6)		2.698(6)
	2.679(6)		2.686(6)
	2.663(6)		2.633(6)
Average	2.656(6)		2.670(6)
Angle of F15-Dy-Cp’	177.3(1)	Angle of F15-Dy-Cp’	175.1(1)

Table S5: Selected Distances (Å) and Angles (°) for one of the molecules in the asymmetric unit of complex **4Dy**.

	Dy1	Dy2
Dy–O1	2.260(2)	2.237(2)
Dy–O2	2.261(2)	2.232(2)
Dy–C(Cp’1)	2.669(5)	2.684(4)
	2.650(5)	2.669(4)
	2.639(4)	2.650(4)
	2.656(4)	2.671(4)
	2.681(5)	2.674(4)
Average	2.659(4)	2.669(4)
Dy–C(Cp’2)	2.646(4)	2.671(4)
	2.652(4)	2.677(4)
	2.653(4)	2.666(4)
	2.675(4)	2.668(4)
	2.664(4)	2.668(4)
Average	2.658(4)	2.670(4)
Angle of O1-Dy-O2	74.36(1)	75.37(1)
Angle of Centroid (Cp’1)-Dy-Centroid (Cp’)	127.4(1)	129.9(1)
Dihedral angle of the two Cp’	57.8(1)	49.6(1)

Table S6: Calculated energy levels (cm^{-1}), $\boldsymbol{g}$ (g_x, g_y, g_z) tensors and m_J values of the lowest Kramers doublets (KDs) of individual Dy^{III} fragments of complexes **1Dy**,**2Dy** and **4Dy**.

KDs	**4Dy**						**1Dy**		
	Dy1			**Dy2**			**Dy1**		
	E/cm^{-1}	$\boldsymbol{g}$	m_J	E/cm^{-1}	$\boldsymbol{g}$	m_J	E/cm^{-1}	$\boldsymbol{g}$	m_J
1	0.0	0.091 3.69 15.532	±15/2	0.0	0.2378 0.8919 17.299	±15/2	0.0	0.112 0.139 18.472	±15/2
2	30.0	0.062 3.644 14.552	±1/2	2.96	0.2176 0.804 17.778	±7/2	9.04	1.406 1.680 16.158	±9/2
3	79.3	0.361 0.456 16.174	±7/2	58.2	0.309 0.680 15.544	±5/2	55.8	1.283 2.029 13.392	±13/2
4	114.4	0.404 0.870 15.866	±13/2	124.5	0.431 0.457 16.004	±13/2	115.5	0.070 1.219 15.204	±3/2
5	169.4	4.160 5.363 10.411	±11/2	185.3	3.793 5.158 11.289	±11/2	161.9	3.502 5.736 11.753	±11/2
6	223.9	2.505 4.039 11.134	±9/2	241.1	2.507 4.081 11.265	±9/2	209.7	2.000 4.168 10.573	±7/2
7	291.6	0.576 1.164 15.767	±3/2	317.3	0.461 0.912 15.780	±3/2	288.8	0.345 0.465 15.496	±5/2
8	473.7	0.046 0.076 19.623	±5/2	540.3	0.0445 0.0814 19.571	±1/2	499.9	0.052 0.086 19.635	±1/2

KDs	**2Dy**								
	Dy1			**Dy3**			**Dy2**		
	E/cm^{-1}	$\boldsymbol{g}$	m_J	E/cm^{-1}	$\boldsymbol{g}$	m_J	E/cm^{-1}	$\boldsymbol{g}$	m_J
1	0.0	1.082 3.705 15.419	±15/2	0.0	0.074 0.261 19.390	±15/2	0.0	0.533 0.741 17.744	±15/2
2	18.2	1.742 2.366 12.839	±5/2	112.9	0.887 1.454 18.023	±1/2	33.6	1.084 2.908 14.459	±7/2
3	68.5	0.123 2.123 12.862	±13/2	168.9	0.166 0.727 16.106	±13/2	75.3	2.053 5.314 9.468	±13/2
4	103.6	0.262	±3/2	242.3	8.212	±9/2	113.5	1.801	±9/2

		2.462 14.200			7.751 4.147			5.166 11.134	
5	174.2	3.117 4.252 12.911	±11/2	305.6	10.571 5.646 0.048	±5/2	182.4	1.081 2.859 14.162	±11/2
6	208.1	3.071 5.296 10.194	±9/2	352.0	1.842 3.778 11.414	±7/2	207.3	8.218 7.813 3.220	±5/2
7	255.6	0.707 0.985 15.158	±7/2	415.2	1.466 2.102 14.024	±3/2	242.9	1.132 1.673 14.309	±3/2
8	384.5	0.085 0.164 19.517	±1/2	457.4	0.187 0.935 16.792	±11/2	354.8	0.102 0.218 19.403	±1/2

KDs	**2Dy**		
	Dy4		
	E/cm^{-1}	***g***	m_J
1	0.0	0.078 0.231 19.541	±15/2
2	115.7	0.850 1.066 18.472	±1/2
3	203.8	1.378 1.780 14.294	±13/2
4	246.9	10.163 7.362 2.952	±7/2
5	314.3	1.209 3.535 11.427	±3/2
6	363.6	1.748 2.679 13.285	±9/2
7	400.6	1.439 1.870 13.998	±5/2
8	508.4	0.095 0.210 18.870	±11/2

Table S7: Exchange energies (cm^{-1}) and main values of the g_z for the lowest two exchange doublets of complex **4Dy**, the lowest four exchange doublets of complex **1Dy** and the lowest eight exchange doublets of complex **2Dy**

	4Dy		**1Dy**		**2Dy**	
	E/cm^{-1}	g_z	E/cm^{-1}	g_z	E/cm^{-1}	g_z
1	0.0	38.045	0.0	18.476	0.0	29.751
2	3.0	2.337	1.7	15.304	0.1	37.800
3			1.7	52.240	0.1	39.282
4			1.7	18.468	0.2	34.499
5					0.6	7.830
6					2.3	24.042
7					2.9	27.782
8					4.7	53.707

Figure S1: Variable-field-variable-temperature magnetization measurement for **1Dy**.

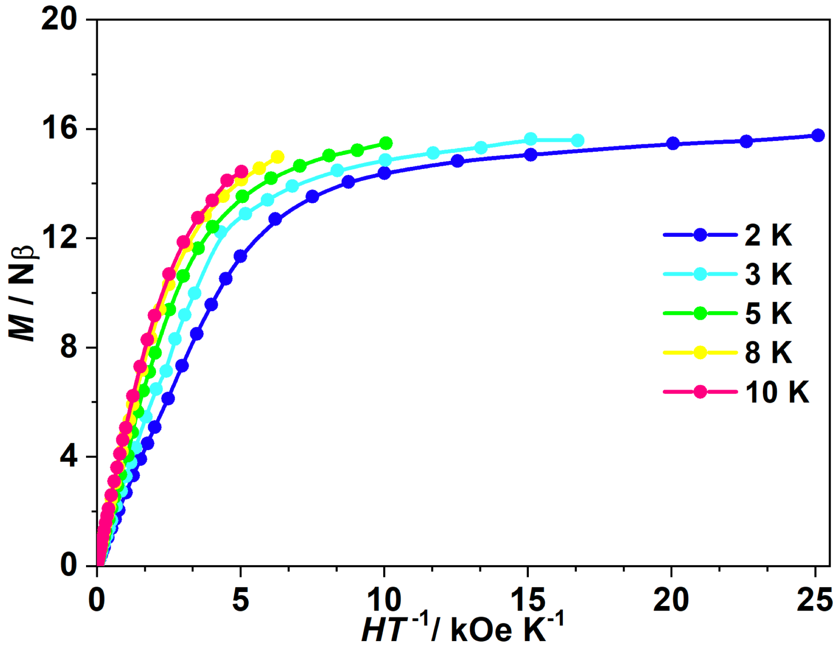

Figure S2: Variable-field-variable-temperature magnetization measurement for **2Dy**.

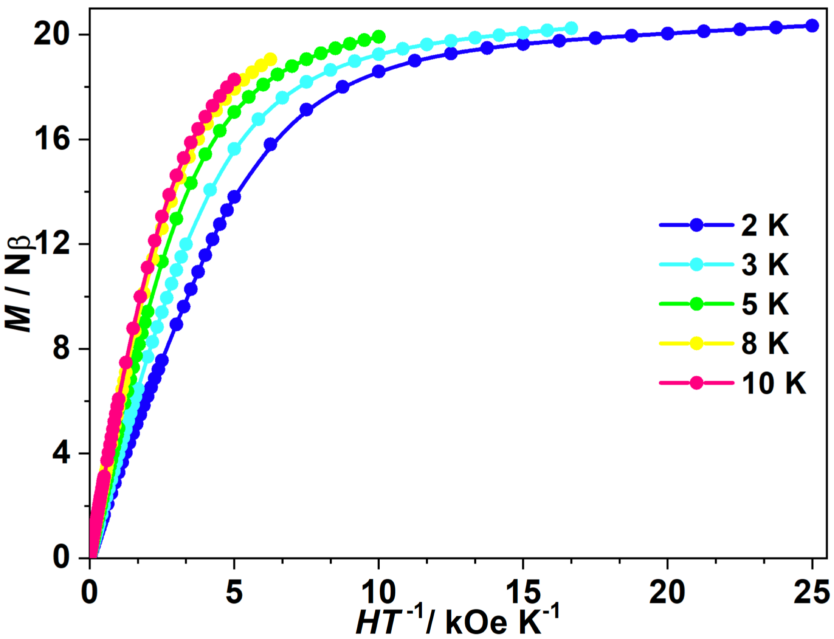

Figure S3: Variable-field-variable-temperature magnetization measurement for **3Dy**.

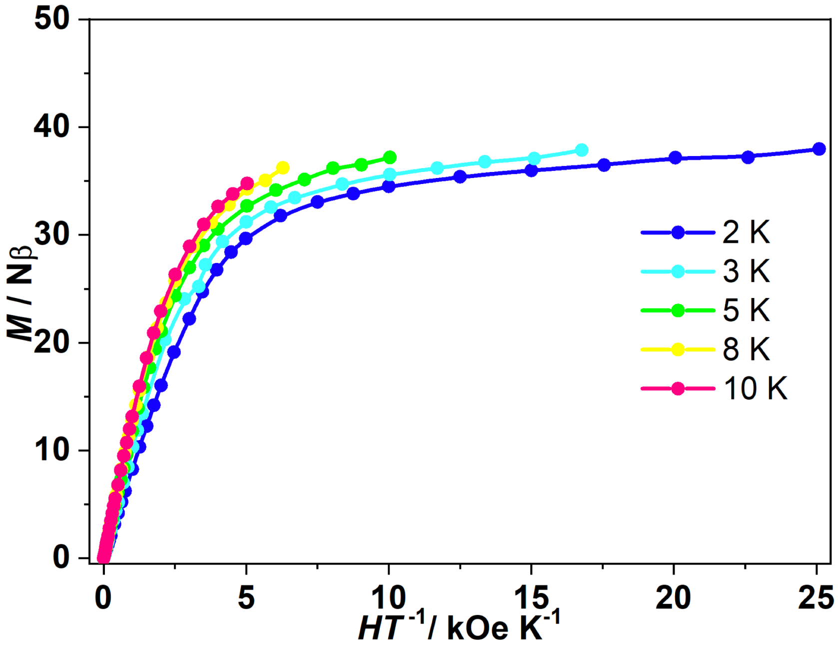

Figure S4: Variable-field-variable-temperature magnetization measurement for **4Dy**.

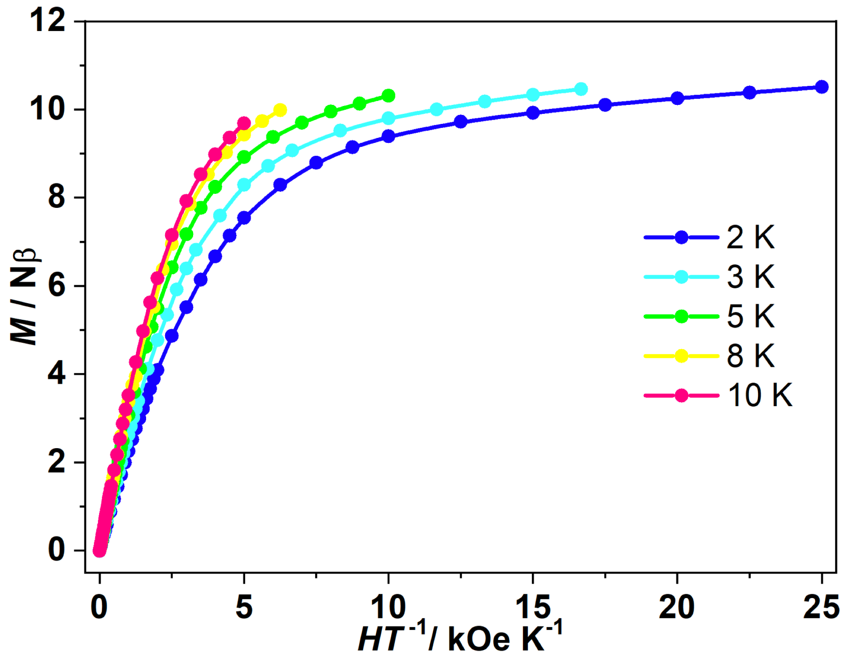

Figure S5 Temperature dependence of ac susceptibility in the absence of dc field for **1Dy**.

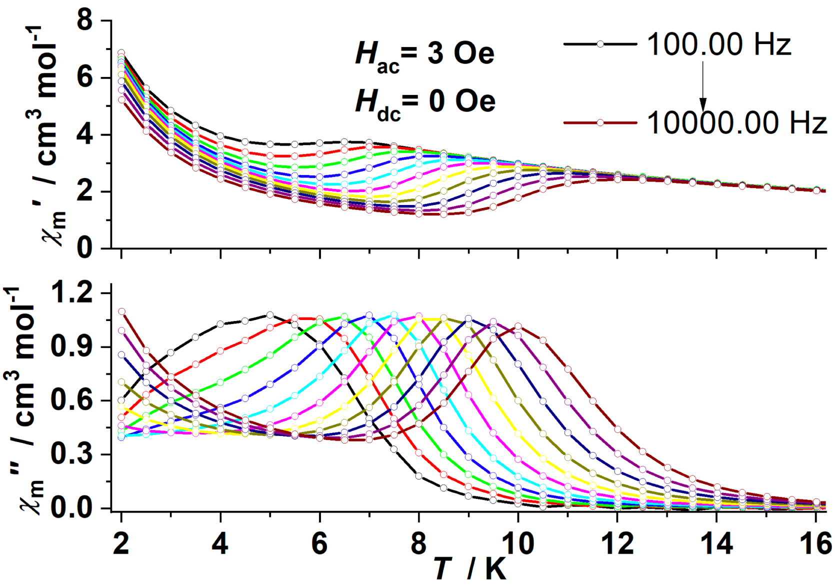

Figure S6: Temperature dependence of ac susceptibility under 1.5 kOe dc field for **1Dy**.

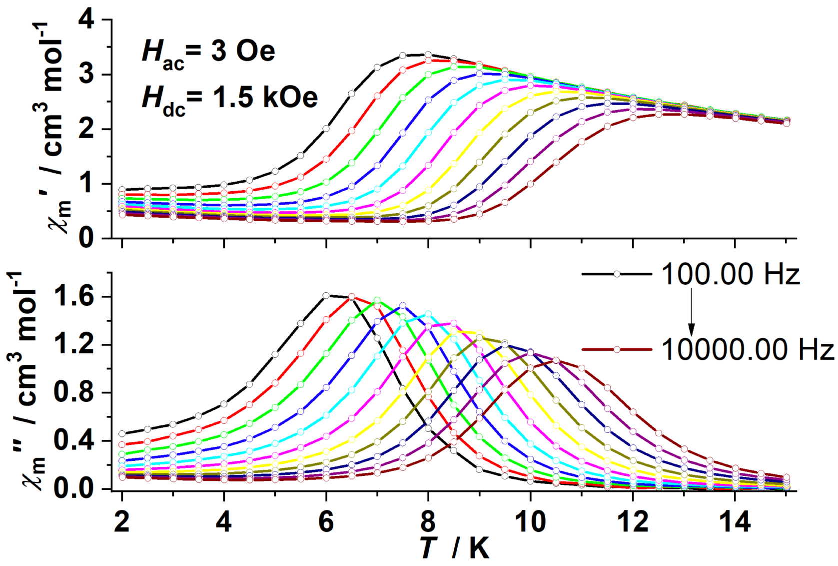

Figure S7 Temperature dependence of ac susceptibility in the temperature range of 2 K to 10 K in the absence of dc field for **2Dy**.

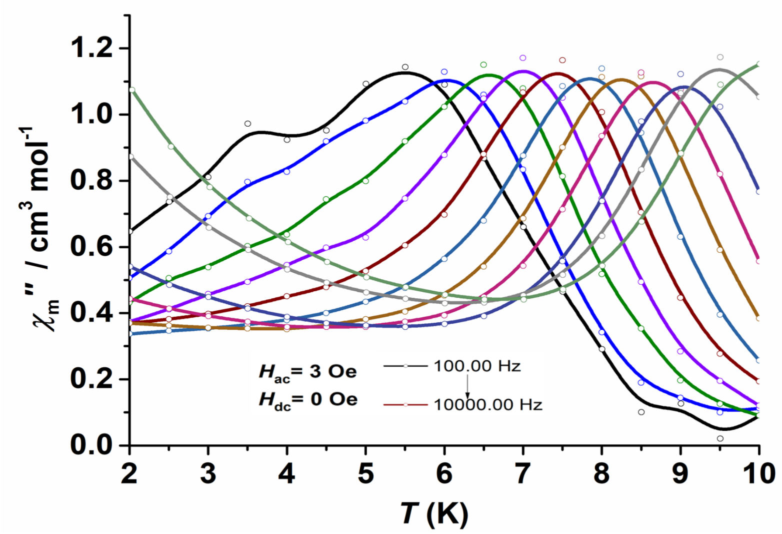

Figure S8: Cole-Cole plots fitting for the determination of the temperature dependence of τ for **1Dy** in the absence of dc field (a) and (b) under 1.5 kOe dc field.

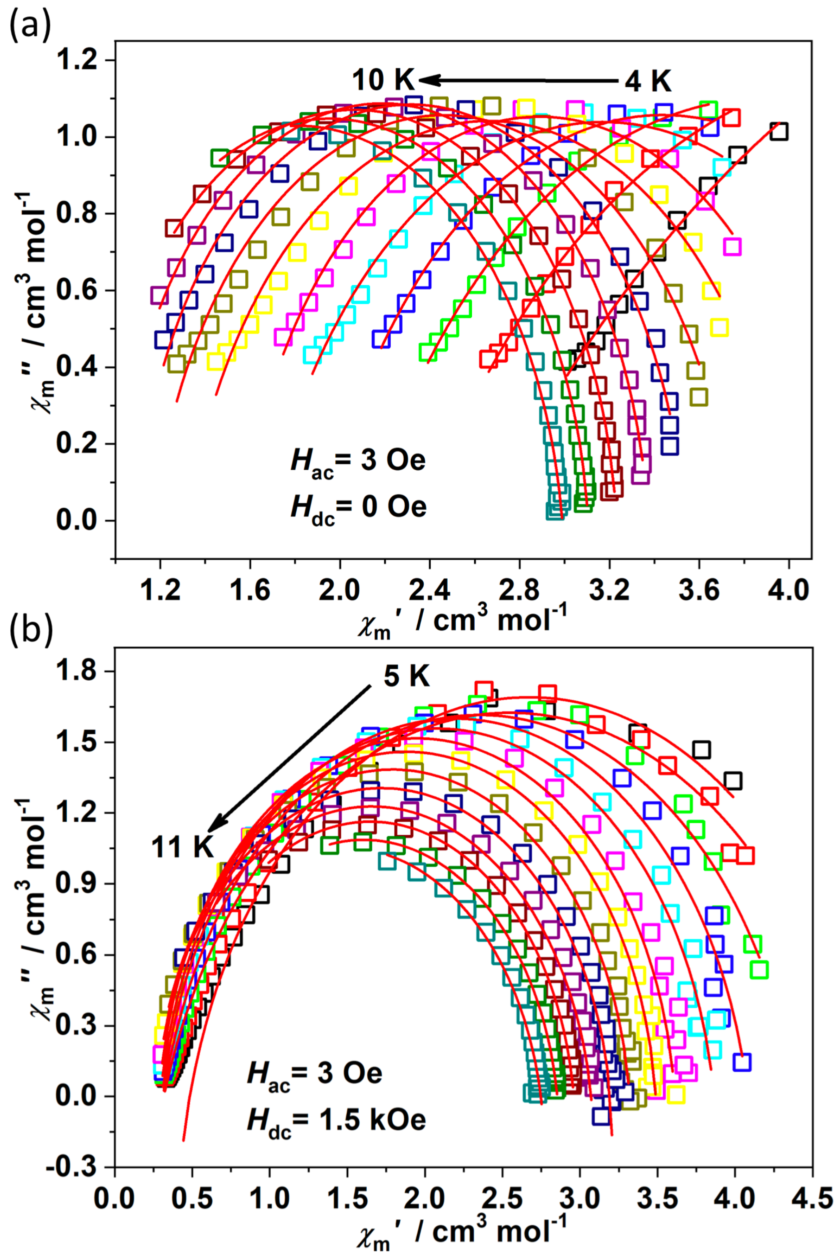

Figure S9: Cole-Cole plots fitting for the determination of the temperature dependence of τ for **2Dy** in the absence of dc field (a) and (b) under 2.0 kOe dc field.

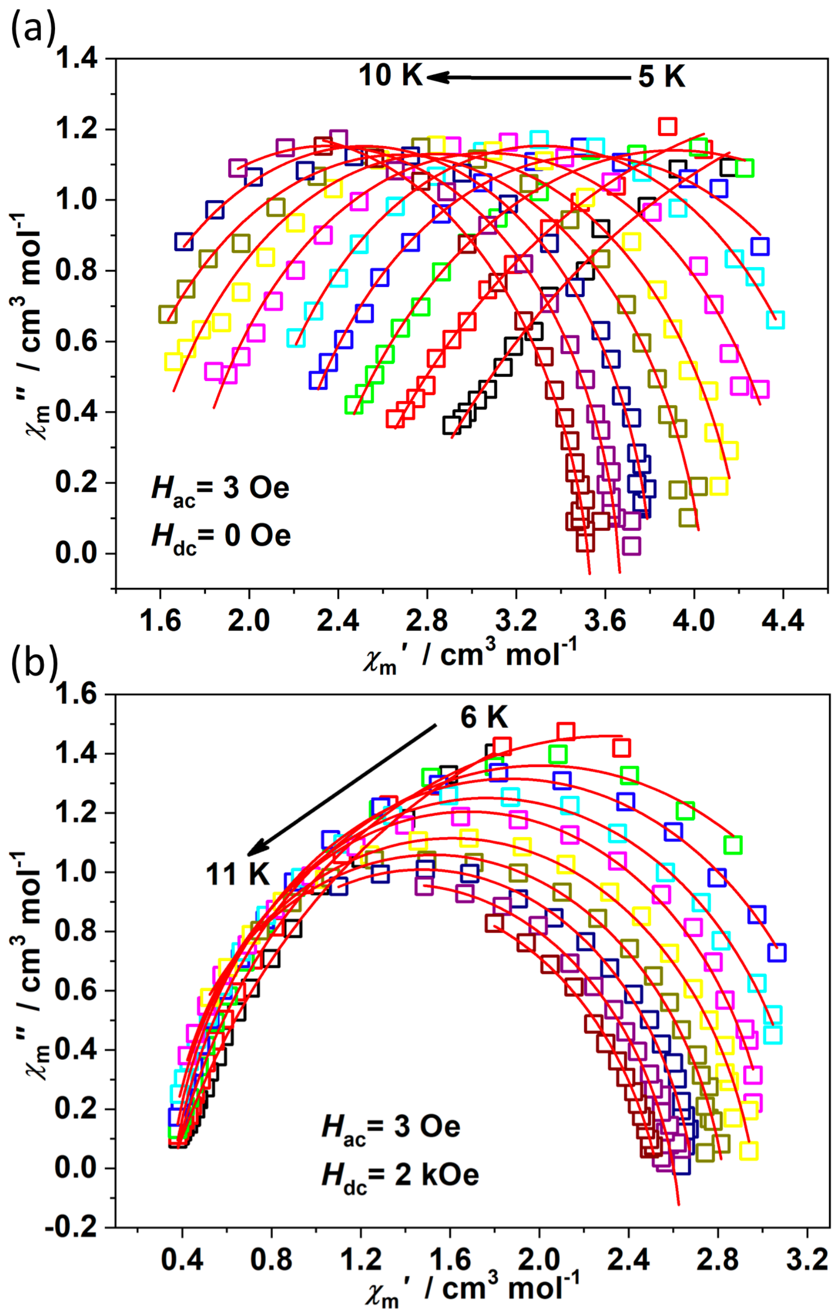

Figure S10: Frequency dependence of ac susceptibility for **3Dy** in the absence of dc field.

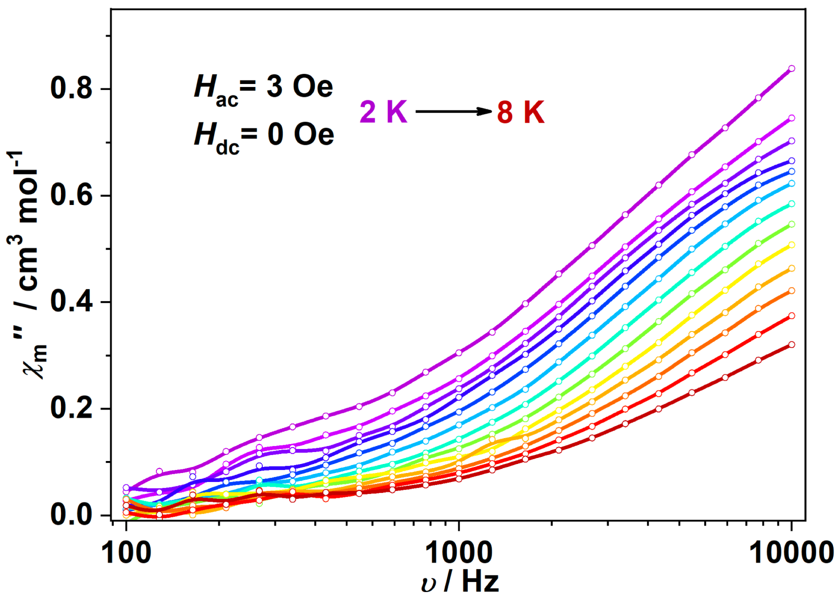

Figure S11. Temperature and frequency dependence of ac susceptibility for **4Dy** in the absence of dc field (a) and under 2.5 kOe dc field (b).

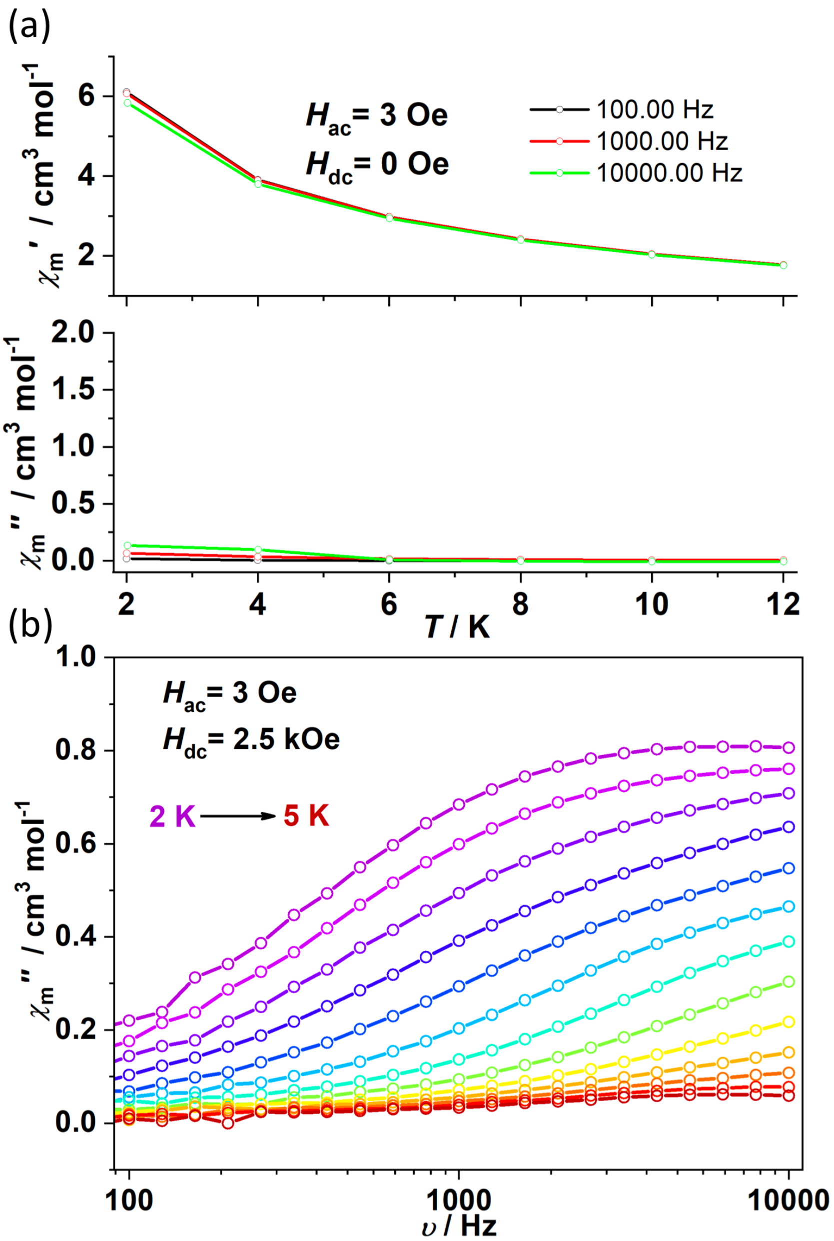

Figure S12: Magnetization blocking barrier for individual Dy^{III} fragments in **1Dy**.

The thick black lines represent the Kramers doublets as a function of their magnetic moment along the magnetic axis. The green lines correspond to diagonal quantum tunneling of magnetization (QTM); the blue line represent off-diagonal relaxation process. The numbers at each arrow stand for the mean absolute value of the corresponding matrix element of transition magnetic moment.

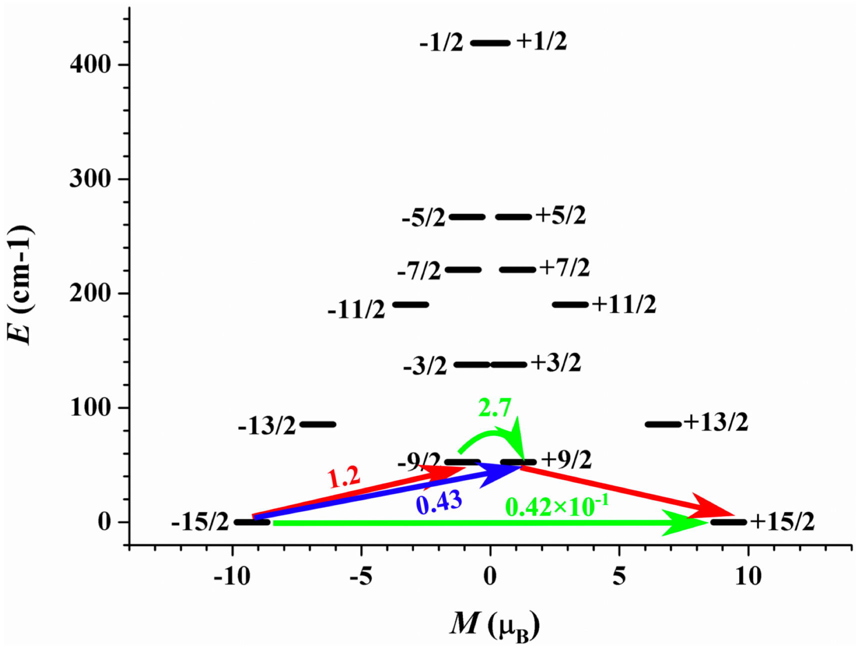

Figure S13: Magnetization blocking barriers for individual Dy^{III} fragments in **2Dy**.

The thick black lines represent the Kramers doublets as a function of their magnetic moment along the magnetic axis. The green lines correspond to diagonal quantum tunneling of magnetization (QTM); the blue line represent off-diagonal relaxation process. The numbers at each arrow stand for the mean absolute value of the corresponding matrix element of transition magnetic moment. (a and b represent Dy1 and Dy2, c and d represent Dy3 and Dy4, respectively)

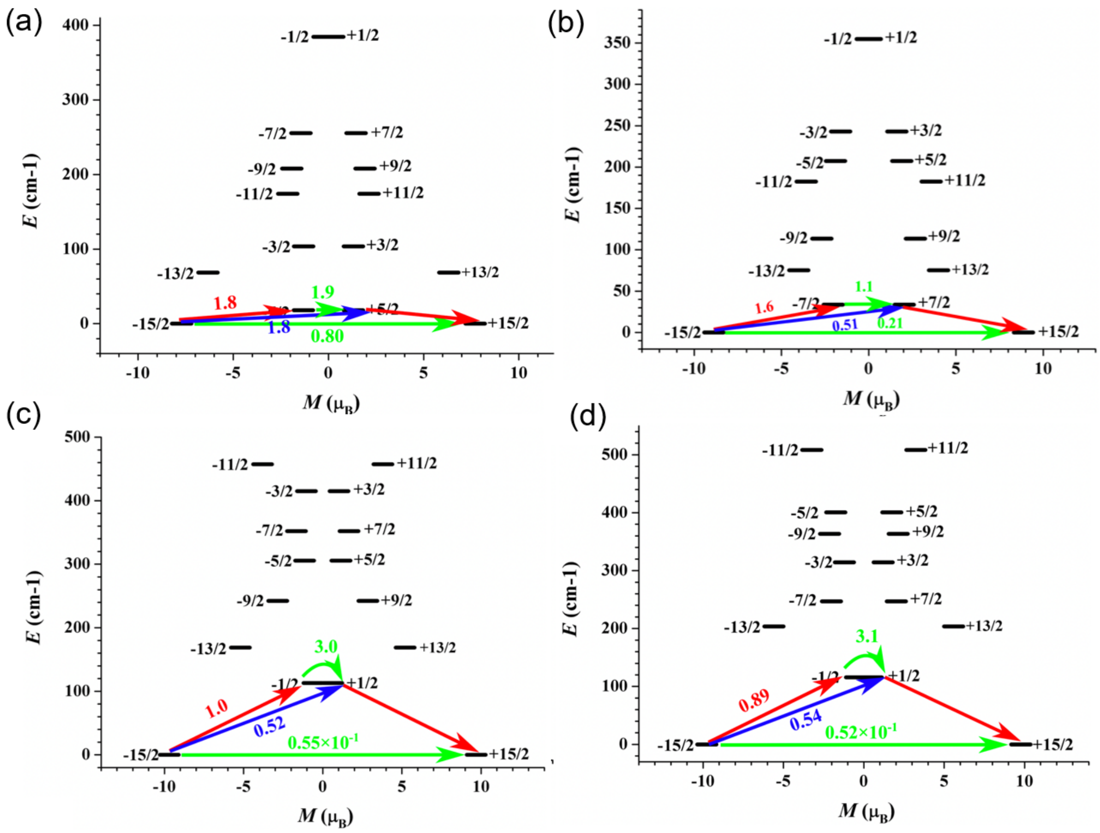

Figure S14: Magnetization blocking barriers for individual Dy^{III} fragments (Dy1 and Dy2) in **4Dy**.

The thick black lines represent the Kramers doublets as a function of their magnetic moment along the magnetic axis. The green lines correspond to diagonal quantum tunneling of magnetization (QTM); the blue line represent off-diagonal relaxation process. The numbers at each arrow stand for the mean absolute value of the corresponding matrix element of transition magnetic moment.

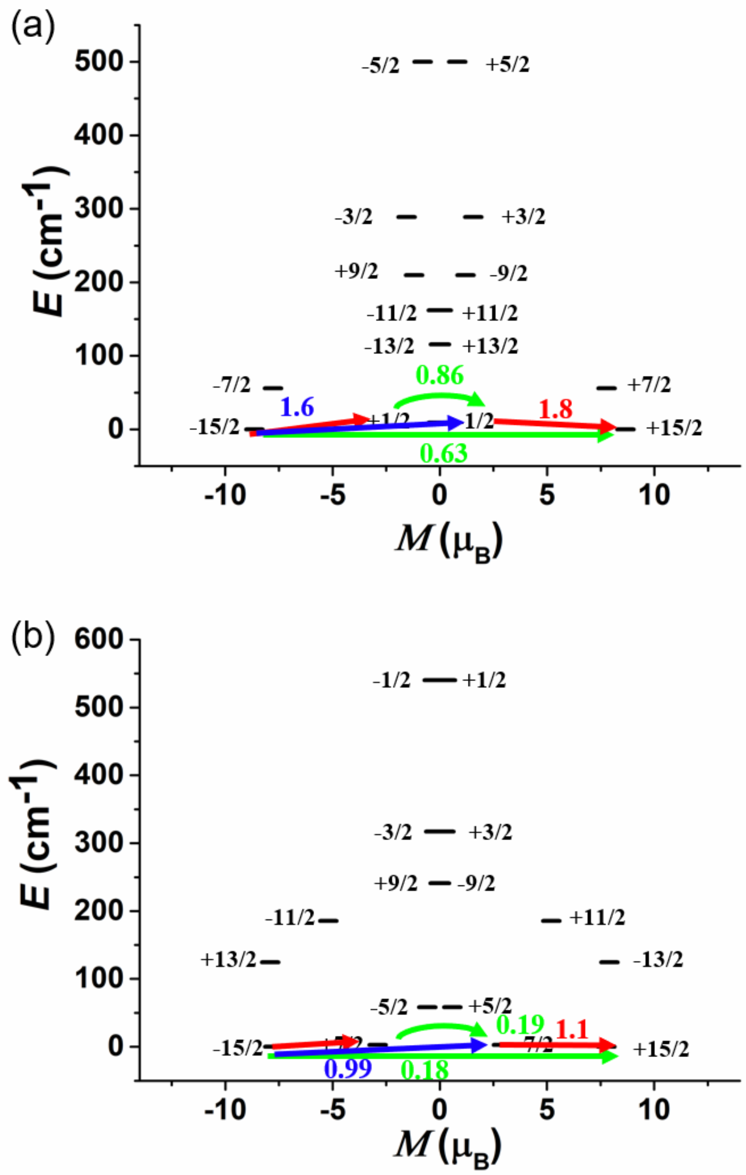

Figure S15: *Ab initio* calculated easy axis for **1Dy**.

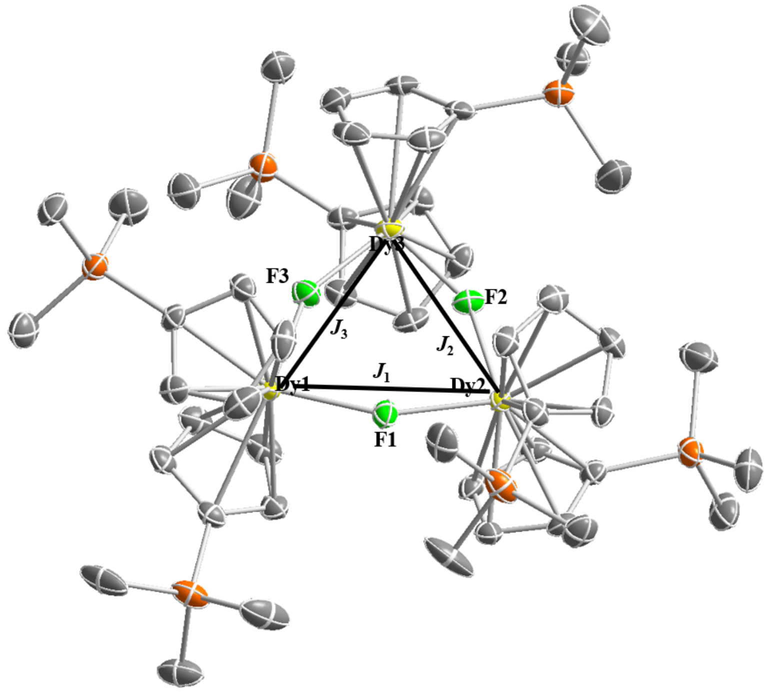

Figure S16: *Ab initio* calculated easy axis for **2Dy**.

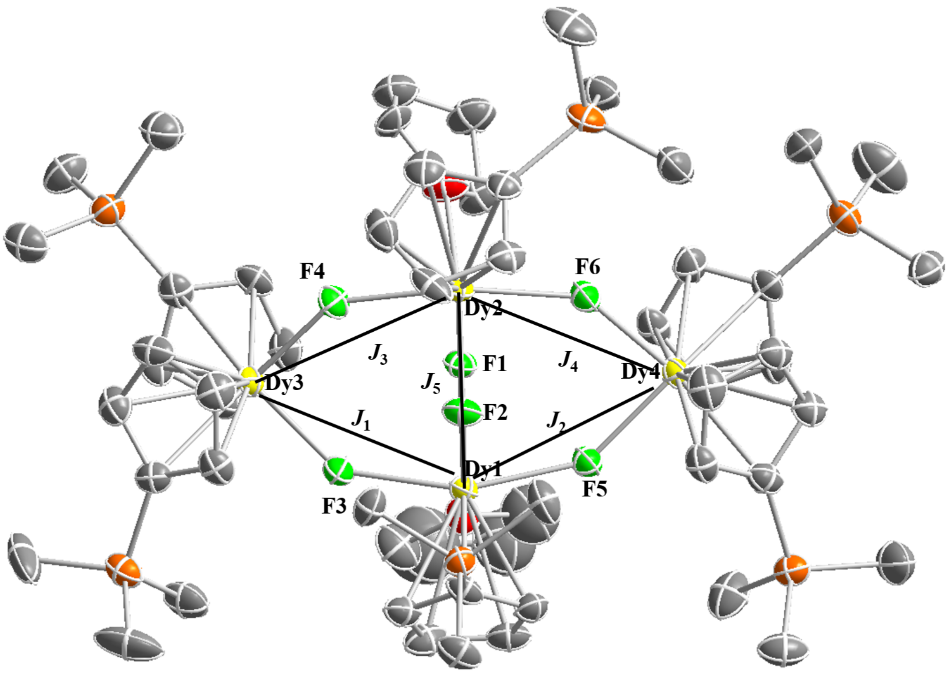

Reference

[1] O. V. Dolomanov, L. J. Bourhis, R. J. Gildea, J. A. K. Howard and H. Puschmann, OLEX2: a Complete Structure Solution, Refinement and Analysis Program. *J. Appl. Cryst*. **2009**, *42*, 339.

[2] L. Spek. Anthony, PLATON SQUEEZE: a tool for the calculation of the disordered solvent contribution to the calculated structure factors. *Acta Cryst.* **2015**. *71*, 9.

[3] G. Karlströma, R. Lindh, P-Å. Malmqvist, B. O. Roos, U. Ryde, V. Veryazov, P.-O. Widmark, M. Cossi, B. Schimmelpfennig, P. Neogrady and L. Seijo, MOLCAS: A Program Package for Computational Chemistry. *Comp. Mater. Sci.* **2003**, *28*, 222.

[4] L. F. Chibotaru, L. Ungur and A. Soncini, The Origin of Nonmagnetic Kramers Doublets in the Ground State of Dysprosium Triangles: Evidence for a Toroidal Magnetic Moment. *Angew. Chem. Int. Ed.* **2008**, *47*, 4126.

[5] L. Ungur, W. V. Heuvela and L. F. Chibotaru, Ab initio Investigation of the Non-collinear Magnetic Structure and the Lowest Magnetic Excitations in Dysprosium Triangles. *New J. Chem.*, **2009**, *33*, 1224.